PHYSICAL REVIEW B VOLUME 28, NUMBER 9 1 NOVEMBER 1983

Superconducting phase transitions in indium/indium-oxide thin-film composites

A. T. Fiory and A. F. Hebard
AT&T Bell Laboratories, Murray Hill, New Jersey 07974

W. I. Glaberson
Rutgers University, New Brunswick, New Jersey 08854
(Received 26 April 1983)

Low-frequency techniques are used to examine the predictions of the equilibrium Kosterlitz-Thouless theory of the vortex-pair unbinding transition in indium/indium-oxide composite superconducting thin films. The renormalized superfluid density obtained from independent measurements of the kinetic inductance and the exponent of the current-dependent resistance are in agreement. At the transition temperature T_c, the critical value of the superfluid density agrees with theory for a finite measurement length. Experimental sensitivity is such that the resistance near T_c, measured to be about 9 orders of magnitude below the normal resistance, is explained by the motion of a single thermally excited free vortex in a superfluid background renormalized by bound-vortex pairs. The corresponding critical magnetic field for flux entry is also measured. The resistance of the thermally excited free-vortex plasma and the correlation length above the transition temperature obey the qualitative prediction of the theory. Nonuniversal constants in the renormalization-group theory are obtained from the experiment and are found to be sample dependent.

I. INTRODUCTION

Phase transitions in thin-film superconductors,[1–11] Josephson-coupled superconducting arrays,[12–15] and in superfluid helium films[16–24] have received a great deal of attention because of the evident applicability of the theory of Kosterlitz and Thouless for phase transitions in two-dimensional systems in the same universality class as the X-Y model.[1–4,25–37] The theory applies to these systems because thermal fluctuations are dominated by vortex excitations, which are treated as a neutral two-dimensional Coulomb gas interacting with a logarithmic pair potential. The theoretical problem was solved using renormalization-group techniques. The central result is a phase-transition temperature T_c, below which vortices exist only as bound pairs. In this region the equilibrium order-parameter correlation function decays algebraically with distance. Just below T_c the theory predicts that the equilibrium superfluid density approaches a minimum value with a characteristic $(T_c-T)^{1/2}$ temperature dependence.[33] There is a vortex-pair unbinding transition at T_c, where a neutral plasma of free vortices appears, causing the superfluid density to jump to zero. Nelson and Kosterlitz show that the jump should be given by a universal quantity which is determined by the fixed point in the Kosterlitz recursion equations.[33] These equations give the length-scale dependence of the renormalized superfluid density and vortex excitation probability due to the screening effect of the thermally excited vortex pairs.

These features of the theory are the results in the limit in which renormalization is extended to infinite lengths. No sharp equilibrium transition is expected when finite lengths accessible to experiment are taken into account.[36] However, one can obtain predictions for the smooth behavior expected in the vicinity of T_c.[4,35] Finite length is introduced experimentally as one of the following: the width of the sample, the frequency-dependent vortex diffusion length, or the current-dependent critical separation for vortex-pair breaking. We review the theoretical formulas in the next section, paying particular attention to these finite-size effects.

The ac measurements of the superfluid transition in liquid-helium films, made by Bishop and Reppy,[18] showed that the jump in the superfluid density agrees with the universality prediction and that a dissipation peak above T_c is explained by vortex excitations. Following a theoretical study by Ambegaokar and Teitel[37] of the dynamics of vortex pairs in an oscillating force field, the experimental data[18] were fitted by the theory with the use of a procedure in which the renormalization process is terminated at a diffusion length $r_\omega=(14D/\omega)^{1/2}$, where D is the vortex diffusivity and ω the experimental frequency.

Prediction by the dynamical theory of a frequency-dependent manifestation of the Kosterlitz-Thouless transition was verified for superconductors, where the complex ac impedance was measured over 5 orders of magnitude in ω.[5,11] Equilibrium behavior was inferred by extrapolating logarithmic frequency dependence to zero frequency. Independently, measurements of the noise spectrum have demonstrated that vortex transport is indeed responsible for the resistance above T_c.[6] The dc resistance measured at temperatures above T_c for a variety of films was presumed to be dominated by the plasma of free-vortex excitations.[7–9] The time constant associated with thermal relaxation in the plasma was found to be short compared to typical measuring times and concluded to be inconsistent with dynamical theory.[7] In liquid helium the vortex plasma was observed as a contribution to thermal resistance which disappears at T_c.[19,20]

The bound-vortex pairs have also been probed by current-induced dynamical pair breaking in superconducting films.[8,13,38] Theory predicts a power-law dependence of electrical resistance upon current, and that the renormalized superfluid density can be determined from the exponent.[4,25] Analogous heat-flow experiments were done in liquid helium.[20,22,24]

New experimental results are reported here which provide a detailed test of the equilibrium theory as it applies to superconducting films. We used low-frequency techniques with both room-temperature and superconducting quantum interference device (SQUID) detectors to study the regime where a dynamical correction for the reorientation of vortex pairs is not required.[35,37] This is accomplished by working at a frequency which is small compared to Dw^{-2}, where w is the width of the sample. We observe a small, activated dc resistance near T_c for small applied currents. The nonlinear resistance observed above a threshold current gives the renormalized superfluid density, which agrees with the results of independent kinetic inductance measurements. Magnetic field study shows a flux-entry field below T_c, owing to the finite area of the film.[2,39–41] The resistance depends sublinearly on magnetic field below T_c and superlinearly above T_c. The free-vortex plasma is observed for $T > T_c$ when the condition $\xi_+ < w$ is satisfied, where ξ_+ is the vortex-pair correlation length, which is proportional to the mean distance between the free vortices.[4,35]

The theory is applied by using measured values of the superconducting parameters, and a consistent fit to the data for $T \lesssim T_c$ is obtained. The temperature dependence of the resistance above T_c, which theoretically is proportional to ξ_+^{-2}, is shown to be given only approximately by the values of ξ_+ obtained from solutions of the Kosterlitz recursion equations.[27,33]

II. KOSTERLITZ-THOULESS THEORY FOR SUPERCONDUCTORS

We briefly mention the theoretical results presented in several theoretical papers,[4,25–35] particularly the treatment of the superconductors case by Halperin and Nelson,[4] and the dynamical theory by Ambegaokar, Halperin, Nelson, and Siggia.[35] The theory is constructed in terms of two parameters: K, the reduced stiffness constant, and y, the vortex excitation probability, also called the vortex activity. These quantities are renormalized by thermally excited bound-vortex pairs. Theory predicts that knowledge of K and y at any given length r can be used to predict behavior at other lengths through a solution of the Kosterlitz recursion equations,

$$\frac{dK^{-1}}{dl}=4\pi^3 y^2 \tag{2.1}$$

and

$$\frac{dy}{dl}=(2-\pi K)y , \tag{2.2}$$

where l is a length parameter defined as $l=\ln(r/\xi_c)$ and ξ_c is the vortex-core size. The connection with experimental quantities is

$$K=n_s\hbar^2/4mk_BT , \tag{2.3}$$

where n_s is the renormalized superfluid density and m is the electron mass. The exponent η for the algebraic decay of the superconducting order-parameter correlation function is related to K by

$$\eta=1/2\pi K . \tag{2.4}$$

Equations (2.1) and (2.2) contain a fixed point which determines T_c and is given by

$$\lim_{l\to\infty} K(l)=2/\pi \tag{2.5}$$

at $y=0$. The temperature dependence near the fixed point is obtained by expanding K and y to first order in $\tau\equiv(T-T_c)/T_c$,

$$K=(2/\pi)+K_0+K_1\tau , \tag{2.6}$$

$$y=y_0+y_1\tau . \tag{2.7}$$

The results can be expressed in terms of a temperature-dependent parameter $X(T)$ which, following the form given by Halperin and Nelson, is given as[4]

$$X(T)=2\pi\,|\,\tau/b\tau_c\,|^{1/2} , \tag{2.8}$$

with

$$b\tau_c=(32y_0y_1-2K_0K_1)^{-1} \tag{2.9}$$

and

$$\tau_c=(T_{c0}-T_c)/T_c . \tag{2.10}$$

The parameters b and τ_c are nonuniversal and are not given by the theory. The parameter τ_c is introduced in anticipation of scaling which involves the BCS temperature T_{c0}.[1] Solutions to Eqs. (2.1) and (2.2) near the fixed point are given in the paper by Ambegaokar *et al.*[35] We summarize the noteworthy features below.

For $T<T_c$ the asymptotic behavior, defined[35] for lengths $l \gg l_- \equiv [X(T)]^{-1}$, is given by the expressions

$$4\pi y(l)=X(T)\exp[-lX(T)/2] \tag{2.11}$$

and

$$\pi K(l)=2+X(T)/2 . \tag{2.12}$$

Right at T_c, the solutions at large l are

$$4\pi y(l)=l^{-1} \tag{2.13}$$

and

$$\pi K(l)=2+l^{-1} . \tag{2.14}$$

Equations (2.8) and (2.12) display the theoretical prediction of Nelson and Kosterlitz[33] that the temperature dependence of the superfluid density contains a square-root cusp. In a finite experimental system, a critical point is not observed because the maximum l is bounded by the width of the sample w.[4,36,40,41] Hence, we introduce an experimental length parameter

$$l_m=\ln(w/\xi_c) , \tag{2.15}$$

and make use of the solutions to Eqs. (2.1) and (2.2) at $l=l_m$. In the present work $l_m\approx 9$. The result is that

$K(l_m)$ and $y(l_m)$ are continuous functions of temperature in the vicinity of T_c. It is also true that the large-l solutions given above are inadequate for $l \sim l_m \sim 9$, since the exact formulas depend significantly upon unknown initial condition ($l=0$) parameters. Direct integration of the recursion relations circumvents this complication.

In order to observe predictions of the static theory, the characteristic time of the measurement must be slow enough for the system to relax under the influence of an external current. For measurements carried out at a frequency ω, the dynamics of vortex-pair polarization fixes an effective value of l given as[33]

$$l_\omega = \tfrac{1}{2}\ln(14D/\omega\xi_c^2) , \tag{2.16}$$

where D is the vortex diffusion constant. Thus dynamical corrections, which were needed in interpreting previous ac experiments, are unnecessary if $l_\omega > l_m$, i.e., when $\omega < 14Dw^{-2}$ is satisifed in the experiment. In contrast, if $l_\omega < l_m$, then bound-vortex pairs contribute to the dissipation as $y^2(l_\omega)$.

Assuming equilibrium conditions are met, therefore, Eqs. (2.11) and (2.13) show a nonvanishing probability $y(l_m)$ for a free-vortex excitation for $T \lesssim T_c$, which implies a small finite resistance. The following expression[4] from the Bardeen-Stephen theory is used to compute the resistance[42]:

$$R = 2\pi\xi_c^2 n_f R_N , \tag{2.17}$$

where n_f is the areal density of free vortices and R_N is the normal-state resistance. This equation is used to evaluate the resistance at all temperatures, including the $T > T_c$ region. The relationship between n_f and $y(l_m)$ is given by

$$n_f = y(l_m)/w^2 . \tag{2.18}$$

In applying the recursion Eqs. (2.1) and (2.2) to our experiment, we implicitly assume their validity over the entire range $l=0-l_m$ for $T \lesssim T_c$. Solutions as a function of l are readily obtained by numerical integration. A numerical solution is necessary because the approximate solutions given above are valid only in the vicinity of $\pi K \sim 2$. We have assumed for our analysis that at the shortest length, $r=\xi_c$ given by $l=0$, the system is an idealized Ginsburg-Landau superconductor, where $K(0) \propto (T_{c0}-T)/T$ and $y(0)=y_0\exp[-CK(0)]$. T_{c0} is the BCS mean-field transition temperature and the constant C is determined by the vortex-core energy. We further assume that $y_0=1$, which is equivalent to taking one available vortex location per unit $2\pi\xi_c^2$ area.[8,32] From a model of a vortex due to Clem[43] we have an estimate that $C=1.0$.

Solutions for $y(l)$ as a function of $K^{-1}(l)$ are displayed in Fig. 1, which was computed from fits to one of our samples (sample G, as discussed further in Sec. VI). The locus of initial conditions $[y(0),K(0)]$ labeled $l=0$ in the figure is an implicit function of temperature. The separatrix curve passes through the fixed point ($K=2/\pi, y=0$) and determines T_c. The locus $l=l_-$ for $T<T_c$, shown as a dashed curve, was computed[35] using $l_- = [2\pi K(\infty)-4]^{-1}$. Predicted equilibrium behavior in the finite sample is shown by the dashed curve for $l=l_m$.

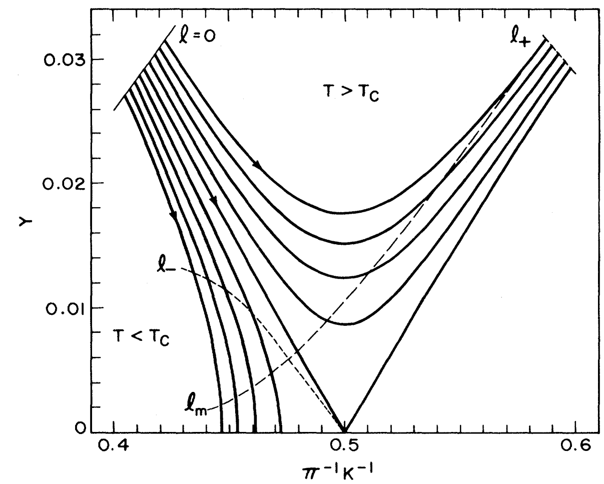

FIG. 1. Theoretical dependence of the parameters $y(l)$ and $K(l)$ of the Kosterlitz-Thouless theory obtained by integration of Eqs. (2.1) and (2.2) using the parameters for sample G in Table I. $l=0$, l_-, l_m, and l_+ curves are discussed in the text.

This latter curve is somewhat sensitive to the $l=0$ conditions, as opposed to the $l \to \infty$ limit, which is insensitive to the initial conditions and is of particular theoretical interest.[33]

We note, as Kosterlitz has observed,[27] that $y(l)$ does not decay to zero at large l for the family of $T > T_c$ curves. The theoretical procedure employed previously in this region is to terminate the renormalization at $l=l_+$ where $y(l_+)=y(0)$, thus defining the two-dimensional correlation length,

$$\xi_+ = \xi_c e^{l_+} , \tag{2.19}$$

from which the density of the free-vortex plasma follows,[4,25]

$$n_f = C_1 \xi_+^{-2} . \tag{2.20}$$

The undetermined numerical factor C_1 is on the order of unity. For the finite sample, there is a temperature T_m, above T_c, where the $l_+ = l_m$ crossover occurs. We have $\xi_+ > w$ in the region $T_c < T < T_m$, so our procedure is to use the $l=l_m$ solution for the computation of the resistance at all temperatures below T_m.

Equation (2.17) is applicable in the $T > T_c$ region for computing the resistance of the free-vortex plasma. Halperin and Nelson have written a formula for the plasma resistance based on the asymptotic behavior near the fixed point, namely

$$l_+ = 2\pi/\chi(T) . \tag{2.21}$$

The constant C_1 was selected by an interpolation procedure, with the result[4] for T close to T_c,

$$R = 10.8bR_N \exp(-2\,|\,b\tau_c/\tau\,|^{1/2}) , \tag{2.22}$$

which involves the same nonuniversal constant b as was given in Eq. (2.8). In Sec. VI we analyze data for the plasma resistance in terms of both Eq. (2.22) and values of l_+ computed by the numerical integration method.

In the foregoing discussion, the measuring current was assumed to be small. Current-induced depairing of the bound vortices occurs when the Lorentz force, proportional to the measuring current I, exceeds the force of mutual attraction in the bound pair, proportional to $r^{-1}K(l)$. Depairing is expressed in terms of a characteristic distance r_c, such that pairs separated by $r > r_c$ are considered as free vortices. The result is[35]

$$r_c = 2\pi c w k_B T K(l_c)/I\phi_0 , \tag{2.23}$$

where $l_c = \ln(r_c/\xi_c)$ and ϕ_0 is the flux quantum. Onset of depairing in a finite film is given by $l_c \approx l_m$ or $r_c \approx w$, which corresponds to a threshold current

$$I_{\text{th}} = 2eK(l_m)k_B T/\hbar , \tag{2.24}$$

which is dependent on w only very close to T_c [see Eqs. (2.14) and (2.15)]. For $r_c \ll w$, the resistance increases with current owing to the current-induced breaking of the bound pairs. We assume that the condition $l_c < l_\omega$ is satisfied so that dynamical relaxation of bound pairs is not an issue here. Halperin and Nelson provide the formula[4]

$$R = R_N(2\pi K - 4)(I/I_0)^{\pi K} , \tag{2.25}$$

where

$$I_0 = w k_B T_c e/\hbar\xi_c . \tag{2.26}$$

Equation (2.25) leads to a power-law dependence of resistance as a function of current when $l_c > l_-$. Pair breaking may also be observed in the regions $l_c < l_-$ for $T < T_c$ and $l_c < l_+$ for $T > T_c$, as discussed further in Sec. VI. We will introduce additional theoretical relationships, as needed, in the following sections describing our experimental results.

III. EXPERIMENTAL PROCEDURES

A. Sample preparation

The indium/oxide films for the experiments were prepared by reactive ion-beam sputter deposition in which an indium target is sputtered by argon ions in the presence of a background partial pressure of oxygen.[44] The substrates were silicon with a thermally grown oxide. Characterizing parameters for our three films are given in Table I. Transmission-electron microscopy has revealed that the structure of these films can range from granular crystalline to mixed amorphous and crystalline, depending upon the oxygen pressure during deposition.[44] Film G is granular and consists of crystalline ~60-Å-diam particles and crystalline In_2O_3. Films A-1 and A-2, produced at higher oxygen partial pressures, contain amorphous indium and some crystalline In_2O_3. Rutherford-backscattering-spectrometry measurements show that the average indium concentration is 60 at. %.

Multiple sample areas were delineated in each film using photolithography and wet-chemical etching. The low-frequency or dc measurements were made on rectangular-strip samples whose dimensions are given in the table. Additional measurements of the kinetic inductance were made for 3-mm-diam circular samples on films G and A-2, which are distinguished with the notation G-C and A-2-C.

The granular films tend to have a sheet resistance which is uniform across the substrate because the resistivity is a slowly varying function of the oxygen partial pressure.[44] For film G the maximum fractional change in sheet resistance per unit length is 6×10^{-3} mm^{-1}. The main effect of sheet-resistance variation is on T_c, since the mean-field BCS transition temperature T_{c0} is close to that of pure indium, 3.4 K.

Amorphous films, on the other hand, have a resistivity which increases with oxygen partial pressure, and the T_{c0}'s which we obtain are significantly depressed with respect to pure In. Presumably, this is an effect of electron localization on superconductivity in high-resistivity materials.[45] We find that the resistance of the amorphous films can be reduced by annealing. This was done for films A-1 and A-2 by placing them under a heat lamp. The anneals took place in air at a temperature of approximately 95 °C. This treatment permits adjusting the sheet resistance so that the phase transition occurs at a temperature convenient for our pumped liquid-helium cryostats. After heat treatment several samples on film A-2 were examined and we found $\Delta T_c/\Delta R \approx 7\times10^{-4}$ K Ω^{-1}. The A-2 sample described in the table was selected from the most homogeneous region on the substrate, where uniformity in sheet resistance is about the same as for sample G. The computed broadening in the resistance transition for sample A-2 is 1.2×10^{-3} K.

B. Measurement techniques

Sample A-1 was measured with room-temperature voltage detectors, and the resistance was obtained from the

TABLE I. Parameters for indium/indium-oxide films. Sample G is granular; samples A-1 and A-2 are amorphous. P_{O_2} is the ambient oxygen pressure during growth, ρ_0 is the resistivity at 300 K of as-grown film, l is the sample length w is the width, R_N is the normal-resistance at 4 K, T_{c0} is the BCS transition temperature, T_c is the Kosterlitz-Thouless transition temperature, $\tau_c = (T_{c0} - T_c)/T_c$ b is the constant in Eq. (2.22), ξ_c is the Ginzburg-Landau coherence distance at T_c, ϵ_c is the vortex dielectric constant at T_c, C is the vortex-core energy factor, and $l_m = \ln(w/\xi_c)$. All films are 100 Å thick.

Film	P_{O_2} (mTorr)	ρ_0 (mω cm)	l (mm)	w (mm)	R_N ($\Omega/\square$)	T_{c0} (K)	T_c (K)	τ_c	b	ξ_c (Å)	ϵ_c	C	l_m
G	0.21	0.97	1.0	0.3	1248	3.404	3.234	0.052	7	428	1.21	4.6	8.9
A-1[a]	0.58	2.96	0.5	0.1	3735	2.29	1.903	0.21	9	150	1.2	4.6	8.8
A-2	0.42	4.0	0.4	0.2	1777	2.62	1.782	0.47	2	304	1.80	2.2	8.8

[a]See also Ref. 38 where R_N, T_{c0}, b, and ξ_c were derived from the data by different methods.

voltage/current ratio. The nonlinear current-voltage curves were recorded by passing through the sample a current obtained from a circuit which multiplies a unipolar square wave by a slow ramp. For samples *G* and *A*-2, the voltage leads were connected to a nulling circuit with an S.H.E. Corporation SQUID detector.[46] The complex impedances were obtained by balancing a bridge operating at an angular frequency of either 100 or 1000 s^{-1}. The nonlinear impedance was measured with a bipolar square-wave current source.

We found sensitivity to weak ambient magnetic fields[47] using the SQUID detector, so special precautions were taken for those measurements. The samples were mounted on a block of Macor ceramic in a vacuum cryostat. The SQUID was operated at 1.1 K while the sample temperature was varied using a heater. A copper Helmholtz coil was used to produce transverse fields. The coil, cryostat, and SQUID were surrounded by an aluminium shield whose superconducting shielding was switched on or off by changing the helium-bath temperature by a small amount. The ambient magnetic field outside the aluminum shield was typically 0.1 mOe, achieved by canceling the ambient laboratory field with a nested arrangement of trim coils, μ-metal shields, and ac de-Gaussing coils. The transverse component of the field applied to the sample was nulled using the Helmholtz coil and a transverse trim coil outside the aluminum shield. The rms field at the sample was 10 μOe or less.

For four-probe impedance measurements, electrical contacts were made by press-contacting indium-coated wires. For the SQUID measurements, superconducting wire was used for the voltage leads, and a 1-$\mu\Omega$ series resistance was added to avoid persistent currents. Thermal cycling seemed to eliminate trapped flux.

More accurate measurements of the kinetic inductance were made by using the 3-mm circles, samples *G-C* and *A*-2-*C*, in a variation of the two-coil mutual inductance technique of our earlier work.[5,48] The sample disc was placed between two astatic-pair coils. The primary coil produces a localized transverse ac magnetic field on the sample. The detector coil was wound from 25-μm-diam

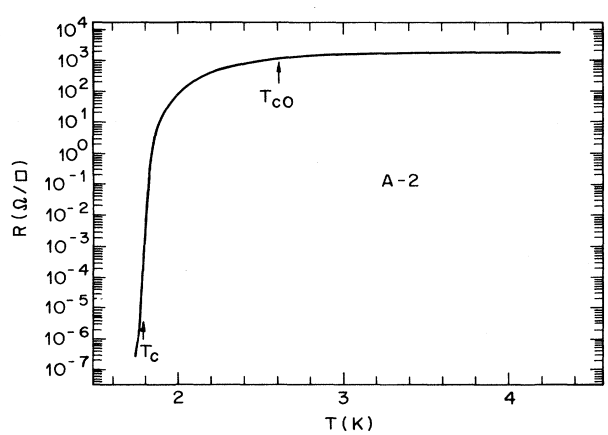

FIG. 2. dc resistance transition for film sample *A*-2. T_c is the Kosterlitz-Thouless temperature and T_{c0} is the BCS temperature.

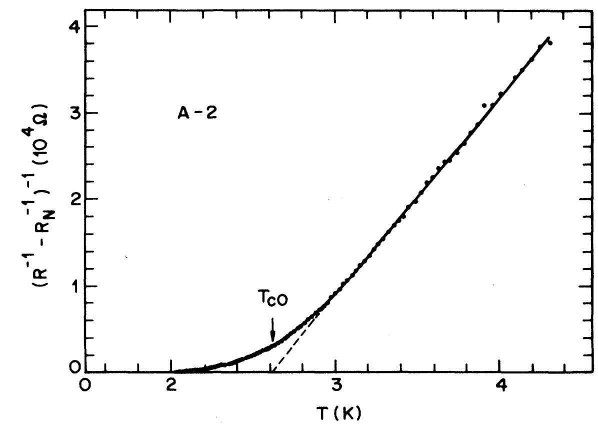

FIG. 3. Paraconductivity contribution to the resistance of sample *A*-2 as a function of temperature. Line is a fit to the Aslamosov-Larkin expression, Eq. (4.1). T_{c0} is the mean-field BCS temperature.

copper wire coated with Pb-Bi-Sn superconductor and connected to the SQUID detector. The complex sheet impedance is computed from the perturbation of the mutual impedance as described previously.[48]

IV. RESISTANCE FOR $T > T_{c0}$

All samples show a negative temperature coefficient of resistance from 8 to 370 K, as is generally found for high-resistivity metals.[45] We are particularly interested in the region just above T_{c0}, where the temperature coefficient is positive. Here the conductance of the films, enhanced by fluctuations of nucleating superconductivity, should be describable by the theory of Aslamasov and Larkin for paraconductivity effects in two dimensions.[49] The theoretical functional form is

$$R^{-1}=R_N^{-1}+R_0^{-1}/(T/T_{c0}-1)\ , \tag{4.1}$$

where R_N is the normal resistance, $R_0=e^2/16\hbar=6.58\times10^4\ \Omega/\square$, and T_{c0} is the BCS mean-field transition temperature.

The resistance transition for sample *A*-2 is shown in Fig. 2. We have fitted Eq. (4.1) to the temperature region between 3 and 5 K in order to find T_{c0} and R_N. In principle these parameters may be temperature dependent owing to the activated contribution to the normal resistance. A three-parameter fit, where R_0 is also varied, provides an experimental value for R_0. Results for sample *A*-2 are shown in Fig. 3, and we obtain $R_0=6.0\times10^4\ \Omega/\square$. Fixing R_0 at the theoretical value changes T_{c0} by -0.03 K. For sample *G*, the best fit is obtained for $R_0=4.6\times10^4\ \Omega/\square$. For sample *A*-1, R_0 could not be meaningfully varied in a three-parameter fit because of the large activated resistance, so R_0 was held at its theoretical value. The results for R_N and T_{c0} are collected in Table I.

V. KINETIC INDUCTANCE $T \lesssim T_c$

At low temperatures, the impedance is dominated by kinetic inductance[5]

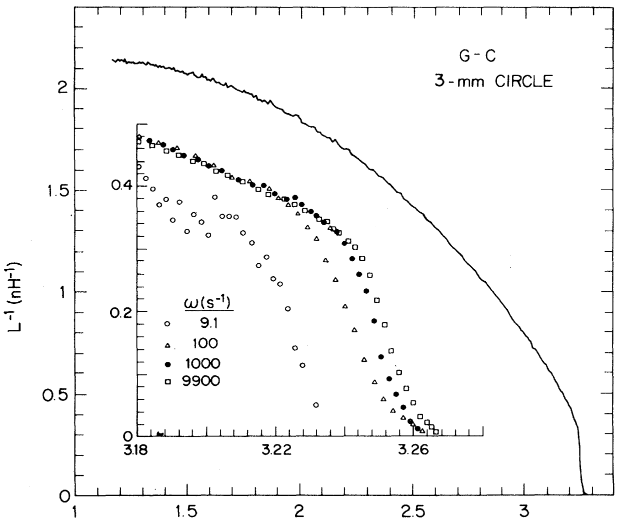

FIG. 4. Inverse kinetic inductance vs temperature for circular film sample *G-C* at $\omega = 10^3$ s^{-1} (solid curve). Inset: dependence near the transition at given frequencies.

$$L_k = m/n_s e^2 ,\tag{5.1}$$

which can also be written in terms of the two-dimensional screening length[39]

$$\Lambda = mc^2/2\pi n_s e^2 ,\tag{5.2}$$

to give

$$L_k = 2\pi\Lambda/c^2 .\tag{5.3}$$

For obtaining the temperature dependence of the film-sheet inductance L, the two-coil contactless method has more sensitivity and accuracy than the four-probe contact method. We plot the inverse kinetic inductance obtained for 3-mm-diam samples *G-C* and *A-2-C* in Figs. 4 and 5, respectively.

The temperature range where L^{-1} drops to zero is the critical region near T_c. Figure 4 shows that some frequency dependence is observed in the vicinity of T_c, as expected theoretically. The location of T_c may be estimated by using the theoretical behavior at $T = T_c$, Eq. (2.14), substituting $l = l_\omega$ as given by Eq. (2.16). The result is

$$\pi\hbar^2/4L_k e^2 k_B T_c = \pi K(l_\omega) = 2 + l_\omega^{-1} .\tag{5.4}$$

In Sec. VI we determine that the vortex diffusion length at T_c is 0.09 cm for $\omega = 1000$ s^{-1} and $l_\omega = 10$. Thus for sample *G-C*, $L_k = 3.6$ nH at $T_c = 3.25$ K, and for sample *A-2-C*, $L_k = 7.4$ nH at $T_c = 1.68$ K. We were unable to observe equilibrium behavior (frequency independence) in sample *G-C* even though the diffusion length is larger than the film diameter at the lowest ω in Fig. 4. For sample *G-C* we were unable to completely eliminate the ambient magnetic field, which introduces a number of free vortices (approximately four). The transition in sample *A-2-C* is broadened by comparatively large film inhomogeneity. In all cases, the experiment is not limited by the finite value of Λ,[4,36] which is about 0.5 cm at $T = T_c$.

It is evident from inspection of Figs. 4 and 5 that the $n_s \propto T_{c0} - T$ temperature dependence one might expect from Ginzburg-Landau theory does not describe the data because of the pronounced curvature at low temperatures. For sample *G-C*, we have taken the nonlinearity into account with a polynomial fit and obtain $T_{c0} = 3.43 \pm 0.02$ K by extrapolation through the critical region. Thus we find that extrapolation of paraconductivity ($T_{c0} = 3.40$ K) and the kinetic inductance give consistent results. The temperature dependence of the data may be compared to the dirty-limit formula[1]

$$L_k^{-1} = \frac{c^2}{2\pi\Lambda(T)} = 69.7 \frac{kT_{c0}}{hR_N} \frac{\Delta(T)}{\Delta(0)} \tanh\left[\frac{\Delta(T)}{2k_B T}\right] .\tag{5.5}$$

With the use of the values of R_N and T_{c0} given in Table I for sample *G*, Eq. (5.5) predicts that L_k^{-1} asymptotically approaches a maximum of 1.96 nH^{-1} at low temperature, which may be compared to the apparent leveling of our experimental curve for sample *G* at 2.15 nH^{-1}. Thus the change in R_N over the temperature interval from 1 K to T_{c0} is only about 5%. An accurate check for sample *A-2-C* is not possible since L^{-1} changes more rapidly with temperature at our lowest measuring temperature.

For the remainder of the paper, we concentrate on results obtained on the comparatively smaller samples, which are *G*, *A*-1, and *A*-2. Complex impedance measurements on samples *G* and *A*-2 were taken with the direct-contact four-probe technique. A small contribution to the measured signal which comes from the mutual inductance between the current and voltage leads was subtracted. This correction was determined by assuming that the kinetic inductances of strip and circular films are the same at $T \sim 1$ K. There is also a negligible geometrical contribution. In contrast to the data near T_c for the circular films, there is no significant dependence of R and L on frequency, which was varied between 16 and 160 Hz, to an accuracy of about 5%. Theoretically, this is expected for samples where $l_m < l_\omega$. Most of the data were taken at 160 Hz, where a better signal-to-noise ratio is obtained.

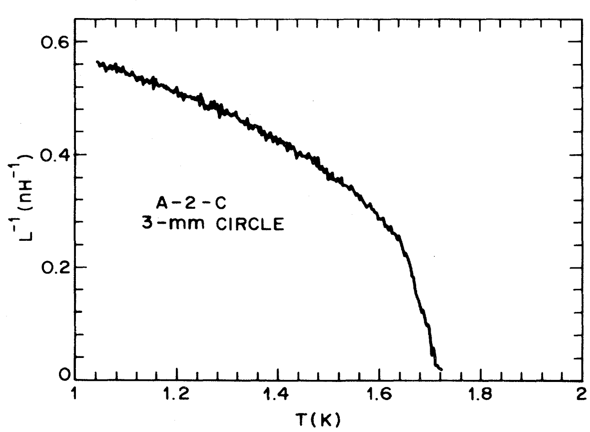

FIG. 5. Inverse kinetic inductance vs temperature for circular sample *A-2-C* at $\omega = 10^3$ s^{-1}.

VI. CRITICAL REGION $T \sim T_c$

A. Magnetic field dependence

The vortex diffusion coefficient in a superconducting film is obtained from the magnetic field dependence of the flux-flow resistance[47]

$$D = Rc^2 k_B T / B\phi_0 \ . \tag{6.1}$$

An implicit assumption here is that the free-vortex density is proportional to the magnetic field,

$$n_f = B/\phi_0 \ . \tag{6.2}$$

Minnhagen's theoretical treatment of the analogous problem of the charged two-dimensional Coulomb gas[41] shows that the linear dependence of Eq. (6.2) holds at $T = T_c$. For $T < T_c$ there is a critical field for flux entry. The magnetic field dependence is faster than linear because of the screening of the interaction between bound pairs by the externally generated vortices. For $T > T_c$ the presence of thermally excited free vortices yields a sublinear dependence of n_f on the external field.

Experimentally, we find that the resistance is independent of current for low currents, so that the critical current is zero. There is no pinning-effect threshold for flux flow. Fisher[50] has argued that a random pinning potential will yield an activated diffusion coefficient. Theoretically, we expect *a priori* from Eq. (2.24) to find a threshold current I_{th} of 55 na for the onset of nonlinear resistance which comes from vortex-pair breaking. In our experiments we begin to observe an increase of several percent in the resistance for currents above 20 na at $T = T_c$, which is in reasonable agreement. Figure 6 shows an example of a threshold transition for sample A-2 at a temperature which is 0.01 K below T_c.

Data for the magnetic field dependence of the resistance were taken with a 160-Hz, 18-na current. Some of the results are shown in Fig. 7 for sample A-2. These and other data for A-1 and G show the qualitative features predicted by Minnhagen.[41]

The resistance varies much more rapidly with temperature at low field, a region dominated by activated vortex nucleation, than at high field, where the temperature dependence is dominated by the more weakly activated vortex diffusivity. For a temperature in the vicinity of 1.782 K, there is a factor-of-100 range in H where the magnetic field dependence is linear. We presume from theory, because R is proportional to H, that this temperature is close to T_c. The deviations at low field, where the temperature dependence becomes most pronounced, is expected because of the finite size of the film. We can express finite size in terms of a field $H_0 = \phi_0 / w^2$, which is 5×10^{-4} Oe for sample A-2.

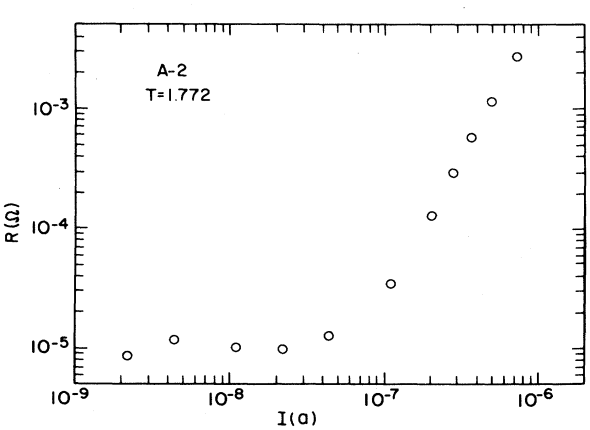

FIG. 6. Resistance (V/I) vs current threshold transition, $T < T_c$, for sample A-2.

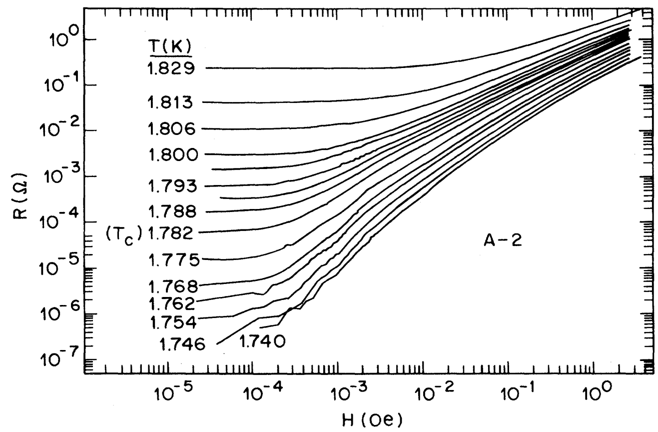

FIG. 7. Resistance vs magnetic field isotherms for sample A-2.

The curves in Fig. 7 tend to merge together at high magnetic field where n_f is dominated by the external magnetic field. The curve identified as being close to T_c is used with Eq. (6.1) to find the vortex diffusion coefficient and using $n_f = B/\phi_0$ in Eq. (2.17) to obtain the coherence distance ξ_c and hence the parameter l_m given in Table I. For fields much above 1 Oe, the formula of Eq. (6.1) no longer precisely describes the data, as some negative curvature is evident. Part of the temperature dependence of the resistance near 1 Oe presumably arises from the activated behavior of D and part from the temperature dependence of the thermally excited vortex density. The diffusion coefficient at T_c is 0.6 cm^2 s^{-1}, which corresponds to a vortex diffusion length[37] of 0.09 cm at our measuring frequency. Thus the absence of frequency dependence near T_c is explained by the sample width being less than the vortex diffusion length. The large magnitude of D in turn suggests that the effects of pinning potentials are comparatively weak near T_c for all the samples.

With the magnetic field dependence of the resistance, we now have the scale factor between R and n_f, the density of free vortices. When we examine the low-field, low-temperature region in Fig. 7, we find that the effective value of n_f is as much as a factor of 50 smaller than w^{-2}, implying that the probability of finding one vortex per unit w^2 area is less than unity.

In an infinite sample the flux-entry critical field H_{c1} vanishes at T_c because of the appearance of thermally excited free vortices at lengths greater than Λ. A convenient and *ad hoc* measure of the flux-entry critical field in our

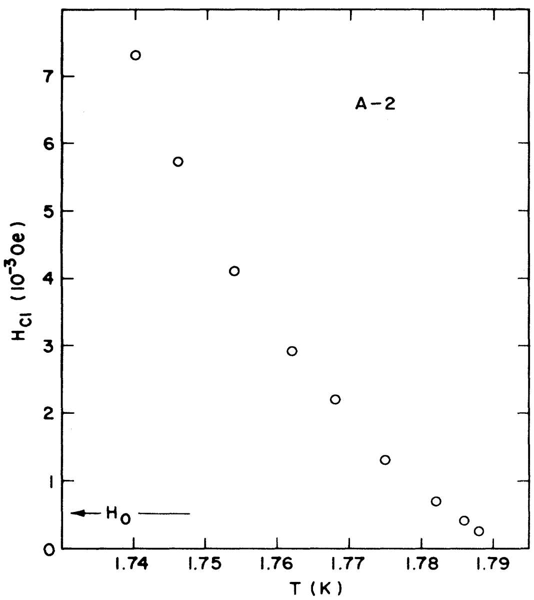

FIG. 8. Critical field H_{c1} vs temperature for sample A-2.

finite sample is the external field which produces one vortex in an area w^2. This corresponds to a threshold resistance of $2\pi\xi_c^2 R_N/w^2 = 2.6\times10^{-4}$ Ω in sample A-2. The values of H_{c1} we obtain in this manner, uncorrected for any temperature dependence of D, are plotted against temperature in Fig. 8. Note that the temperature of 1.784 K, where $H_{c1} = H_0$, is about the same temperature where the resistance is linearly dependent on the field for $H \gg H_0$. Because of the finite value of H_0 there is flux exclusion at all temperatures to about 1.79 K.

Our data are in qualitative accord with Minnhagen's theoretical functions.[41] Minnhagen has defined H_{c1} as an intercept in a plot of n_f vs B. It was not possible for us to use the same procedure because of the nonlinearity of the $R(H)$ curves for $T < T_c$. For $T > T_c$ we can obtain critical exponents from the magnetic field dependence. However, the formulae presented by the theory involve several unknown parameters whose values must be fit. For this

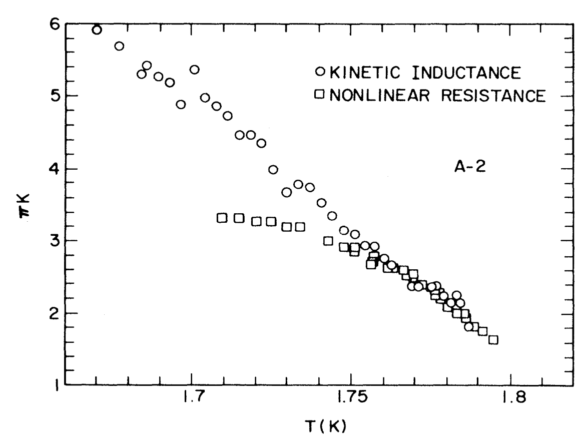

FIG. 9. Reduced stiffness constant πK vs temperature for sample A-2 obtained from kinetic inductance and exponent of current-dependent resistance.

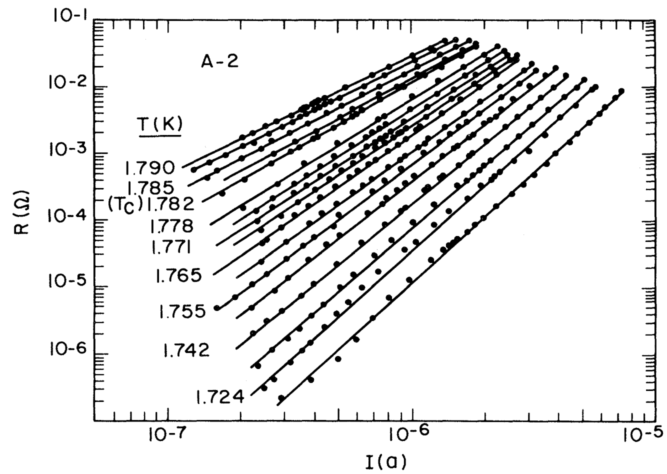

FIG. 10. Resistance-vs-current isotherms for A-2 in the nonlinear region of driving current.

reason, and also because the effect of finite sample size is introduced only approximately in the theory, such fitting results would not be meaningful.

B. Temperature dependence

The renormalized stiffness constant to be compared with theory is computed from data for the kinetic inductance by the relation

$$\pi K(l_m) = \pi\hbar^2/4e^2 L_k k_B T \ . \tag{6.3}$$

The static limit $l = l_m$ applies for the small samples. The quantity $\pi K(l_m)$ is plotted against temperature as open circles in Fig. 9 for sample A-2. A theoretical value of $\pi K(8.8) = 2.11$ at $T = T_c$ is given by Eq. (2.14). The predicted deviation from the precise value of 2, valid in the $l_m \to \infty$ limit, is small and comparable to our experimental accuracy. The temperature where πK crosses 2.11 in Fig. 9 is 1.782 K, with an uncertainty of about ± 3 mK. We find that this is in good agreement with the critical temperature ($T_c = 1.782$ K) identified with the linear $R(H)$ curve in Fig. 7. Data for the kinetic inductance do not extend too far above T_c because the rapidly increasing resistance eventually dominates the impedance. Temperature-fluctuation noise prevents accurate measurement of L_k in this region.

A second procedure for experimentally determining πK is from the exponent of the nonlinear dependence of the resistance on current for $I > I_{\text{th}}$. The family of isotherms for R vs I for sample A-2 is shown in Fig. 10. A similar set of curves has been obtained for sample A-1 (Ref. 38) and sample G. A current range was selected so that the resistance is at least an order of magnitude greater than the linear resistance at small currents. The current corresponds to a vortex-pair-breaking length $r_c \sim 10$ μm, which is an order of magnitude or more smaller than the sample width. Thus the influence of the sample boundaries can be neglected in the analysis of these data.[35,40] To the extent we observe straight lines on our log-log scale plot shows that the dependence of K on the parameter l can be

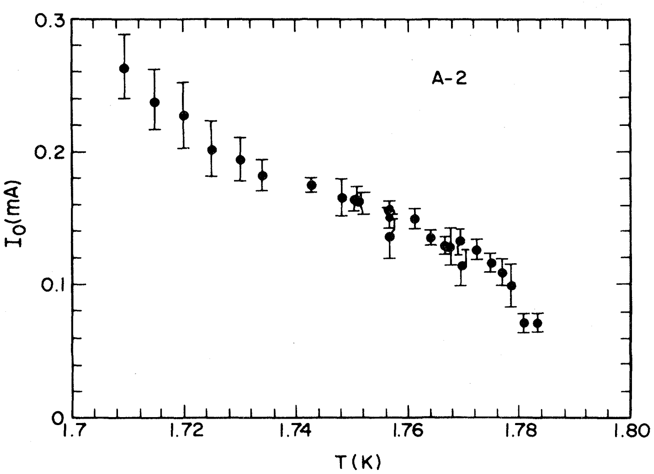

FIG. 11. Scaling current of the power-law resistance for sample A-2.

neglected. For these data we have $l_c = \ln(r_c/\xi_c) \sim 6$. We have fitted Eq. (2.25) to these data and plotted the results for πK as the open squares in Fig. 9. The agreement between the kinetic inductance measurements and nonlinear resistance measurements of πK, compared in Fig. 9, is excellent near T_c, although the deviation below 1.75 K is not readily explained. The scaling current I_0 is plotted against temperature in Fig. 11 for sample A-2. The values of I_0 agree to within a factor of 2 with the expression given in Eq. (2.26), computed with the results for ξ_c obtained from the flux-flow resistance. Since both I_0 and D depend on the vortex-core radius ξ_c, we can also treat the nonlinear resistance and the flux-flow resistance as independent measurements of ξ_c. The comparison is made in Fig. 12, where the temperature dependence is plotted for sample A-1. Results for both measurements show a pronounced increase in ξ_c near T_c. Pinning effects are possibly important, and may influence the flux-flow mobility. Such effects on I_0, which is determined by the vortex-core size, should be much less. A theoretical prediction of enhanced diffusion near T_c by Petschek and Zippelius[51] is in qualitative agreement with this observed increase in ξ_c.

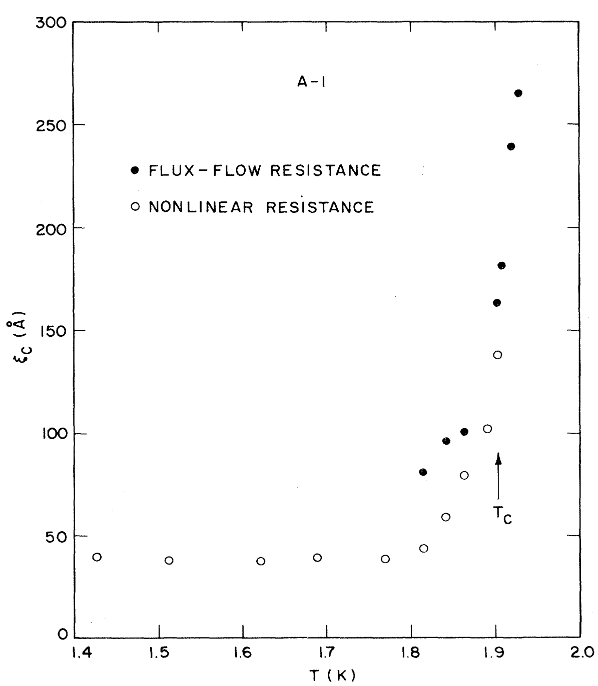

FIG. 12. Vortex-core parameter ξ_c vs temperature obtained from flux-flow resistance (triangles) and from nonlinear resistance (circles).

For temperatures below T_c, we can neglect the length dependence of K if the value of l fixed by the experiment, the smaller of l_c or l_m is larger than the characteristic length l_-. However, this condition cannot be satisfied near T_c because of the divergence in l_-. We calculate a small, 5% difference between $K(l_c)$ and $K(l_m)$ at T_c, although we are not able to resolve it experimentally. However, meaningful results for $K(l_c)$ are obtained by considering the generalization of Eq. (2.25),

$$\pi K(l_c) = \left. \frac{d \ln R}{d \ln I} \right|_{l=l_c}, \tag{6.4}$$

which is valid even for $T > T_c$ if $l_c < l_+$. The small amount of curvature predicted in $\log R$-vs-$\log I$ plots for $T \sim T_c$ is not discernible in the data of Fig. 10 or previous data.[38]

Our procedure for testing the renormalization-group theory is to fit the temperature dependence of $\pi K(l_c)$ by solving Eqs. (2.1) and (2.2) with numerical integration. For this purpose we assume two adjustable parameters: the unrenormalized $K(0)$ parameter, assumed to have a simple $(T_{c0} - T)/T$ temperature dependence, and the vortex-core energy factor C, assumed to be a constant invariant with temperature. The parameter T_{c0} is taken from Table I. The transition temperature T_c is not explicitly an adjustable parameter, and $l_c = 6$ was assumed to be constant. Once a fit for $l = l_c$ is obtained, we find T_c by inspecting the behavior at large l.

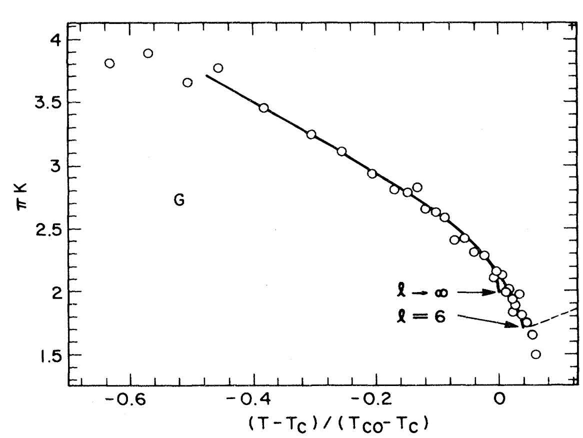

FIG. 13. Reduced stiffness constant vs reduced temperature for sample A-2. Fitted curves are for $l_c = 6$, $l \to \infty$, and $l = l_+$ (dashed curve).

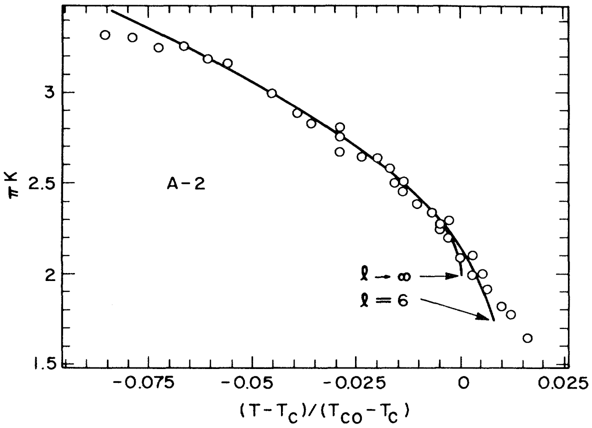

FIG. 14. Reduced stiffness constant vs reduced temperature for sample A-2. Fitted curves are for $l_c=6$ and $l \to \infty$.

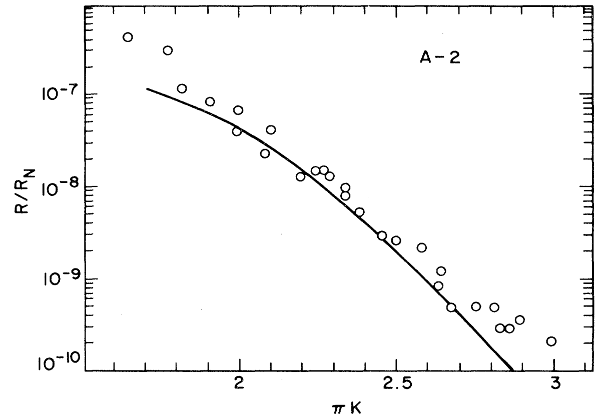

FIG. 16. Normalized resistance vs reduced stiffness constant for sample A-2 and a theory curve, Eq. (6.6), for $l_m=9.0$.

We present the results for samples G and A-2 in Figs. 13 and 14. The temperature scale is written in reduced form as $(T-T_c)/(T_{c0}-T_c)$, so as to test the normalization with respect to the parameter τ_c of Eq. (2.10). For temperatures above T_c, there is a temperature T_m where we truncate the numerical integration because $y(l)$ recovers to its initial value, in accordance with the theoretical prescription. The minimum values of πK displayed in the fits are located at $T=T_m$. The $T>T_m$ region is displayed in Fig. 13 as a dashed curve. The fitting parameters ϵ_c and C are given in Table I, where the dielectric constant at $T=T_c$ is defined in the usual manner,

$$\epsilon_c=\pi K(0)/2 . \tag{6.5}$$

Figures 13 and 14 also show the result for $T<T_c$ when the $l \to \infty$ limit is computed with the same parameters making the fit for $l=l_c$. The difference is significant only very close to T_c, where the square-root cusp is visible and where πK drops discontinuously from 2 to 0. This method of finding T_c, where the values obtained are given in Table I, agrees with the previous analysis of the magnetic field dependence to within experimental accuracy.

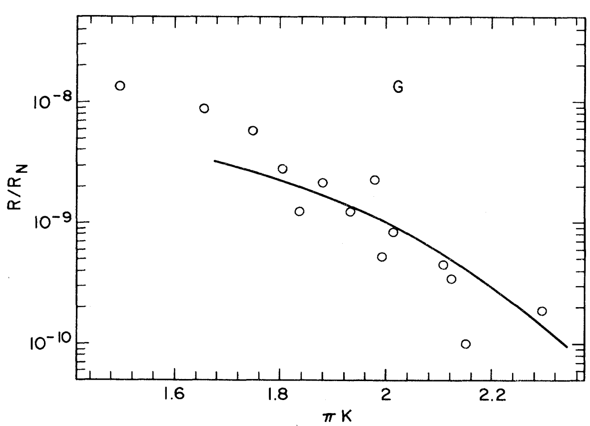

FIG. 15. Normalized resistance vs reduced stiffness constant for sample G and a theory curve, Eq. (6.6), for $l_m=7.3$.

We also use this method to calculate the parameter τ_c.

We now turn to an analysis of the low-current resistance and test whether the magnitude of the resistance agrees with the theory. In the temperature region $T>T_m$, we substitute Eq. (2.18) into Eq. (2.17) and obtain for the dc resistance

$$\frac{R}{R_N}=2\pi e^{-2l_m}y(l_m) . \tag{6.6}$$

Equation (6.6) differs from the dynamical case, where $l_\omega < l_m$, and where the ac resistance is proportional to $\omega y^2(l_\omega)$, i.e., the density of vortex-pair excitations.[35] A nonobvious property of the solution of the recursion equations is that $2\pi e^{-2l}y(l)$, when plotted as a function of $K(l)$, produces a curve which is insensitive to the $l=0$ locus. This relationship is displayed in Figs. 15 and 16. For the data points ordinates were computed from the low-current resistance, and for the abscissa scale the small difference between $\pi K(l_c)$, the measured quantity, and $\pi K(l_m)$, the computed quantity, was neglected. The theory curves (solid lines) in the two figures were computed from Eq. (6.6) for a choice of l_m which best fits the data. Varying l_m in this way shifts the curves in the ordinate direction. The curves terminate on the left at a point corresponding to $T=T_m$ where $l_m=l_+$. These fits correspond to $l_m=7.3$ and 9.0 for samples G and A-2, respectively, which may be compared with the independently determined values of 8.9 and 8.8 given in Table I. We regard this as good agreement between theory and experiment for $T \lesssim T_m$, confirming the theory that dc resistance near T_c arises from a free-vortex excitation in the sample.

The resistance at temperatures above T_m, where we have $l_+ < l_m$, is dominated by the free-vortex plasma. Previous work on superconducting and liquid-helium films has shown that the temperature dependence of Eq. (2.22) gives quite a good fit to data over the broad temperatures range where $R/R_N<0.1$. A fit for sample A-1 is given in Ref. 38. The fitting parameters b are given in Table I. For sample A-2 the value given is approximate because of systematic deviation from Eq. (2.22). The scaling method of the next paragraph gives a better fit to the

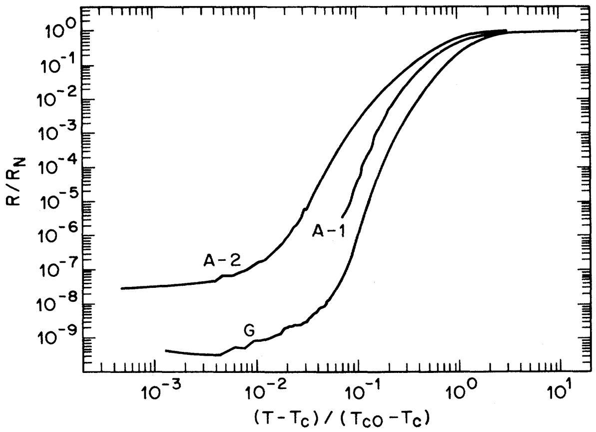

FIG. 17. Comparison of normalized resistance vs reduced temperature for three samples.

A-2 data. The parameter b varies among the samples, as shown by the results in Table I. This was noted for earlier work by Abraham *et al.*[14] Further display of the failure of τ_c scaling is shown in Fig. 17, where the three samples are compared in plots of R/R_N as functions of τ/τ_c. The plots do not superimpose. This implies that the superconducting transition does not obey a simple scaling law with normal resistance, as originally proposed by Beasley, Mooij, and Orlando.[1]

Following a suggestion of Minnhagen[10] that the temperature scaling should include the Ginzburg-Landau temperature dependence of the underlying superfluid, we have also tested the dependence of R/R_N on a parameter X, given by

$$X=\frac{T-T_c}{T_{c0}-T}\ , \tag{6.7}$$

and found that universal scaling is not obeyed in this scheme either. However, it is instructive to plot the data in a manner which produces a straight line if the asymptotic behavior for $X<1$ is to be tested. We choose a method which produces a straight-line plot and which permits displaying the large dynamic range in R/R_N and X. If we take $C_1=1$ in Eq. (2.20) then Eq. (2.22) can be rewritten as

$$[\ln(2\pi R_N/R)]^{-1}=(bX)^{1/2}\ . \tag{6.8}$$

The quantity expressed in Eq. (6.8) is $(2l_+)^{-1}$. Presenting the data in this manner in Fig. 18, we find that the square-root law of the theory is applicable in a limited interval, as shown by the dashed lines passing through the data curves. For temperatures too close to T_c, the divergence in l_+ is cutoff at l_m, while at high temperatures, for $R/R_N \gtrsim 0.1$, the asymptotic formula is not expected to apply. Figure 18 also shows that the X parameter does not produce a universal plot for the two samples shown, and therefore such a dependence does not confirm universality.

A more critical test of the theory is to compute l_+ directly from the renormalization procedure as discussed in Sec. II using the same constants which fit the data for $T \lesssim T_c$. However, in order to compute the resistance, we must assume a value for the unknown constant C_1. Our procedure is to choose a formula which makes R continuous at the quasitransition which occurs at T_m. Thus we use

$$\frac{R}{R_N}=2\pi e^{-2l_+}y(l_+)\ , \tag{6.9}$$

where in this scheme $y(l_+)=y(0)$. The computed results of this procedure show that the $\tau^{-1/2}$ dependence of l_+ given by Eq. (2.21) is obeyed in the rather restrictive interval $\tau/\tau_c \lesssim 10^{-2}$ just above T_c.[10] At higher temperature l_+ decreases more rapidly than $\tau^{-1/2}$, eventually going to zero at $\tau=\tau_0$, which corresponds to the point where the extrapolated $l=0$ and l_+ curves in Fig. 1 meet,

$$\frac{\tau_0}{\tau_c}=\frac{\epsilon_c-1}{\epsilon_c+\tau_c}\ . \tag{6.10}$$

This corresponds to $\pi K(0)=2$. Although Eq. (6.10) gives

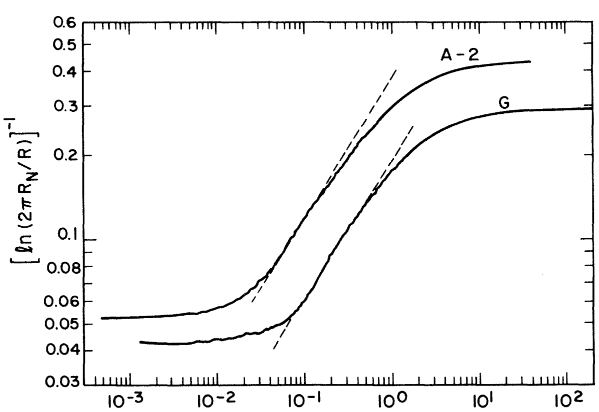

FIG. 18. Plot of reduced resistance on the universal temperature scale parameter, Eq. (6.7). Dashed curves are fitted according to Eq. (6.8).

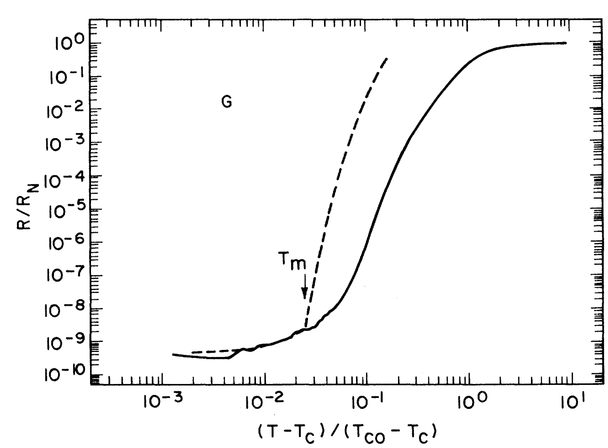

FIG. 19. Experimental (solid curve) and theoretical (dashed curve) dependence of normalized resistance on reduced temperature for sample G. Theory for $T<T_m$ given by Eq. (6.6) and for $T>T_m$ by Eq. (6.9). T_m marks $l_m=l_+$.

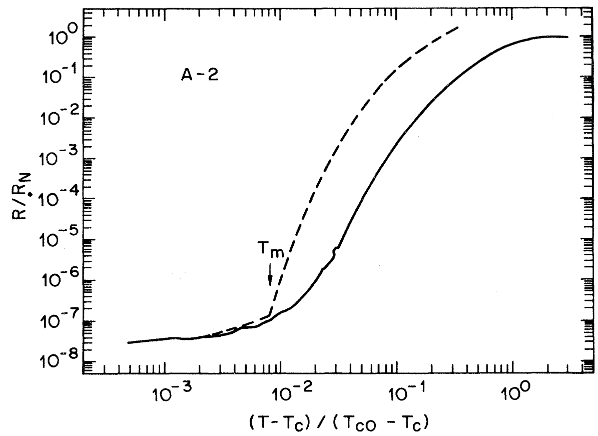

FIG. 20. Experimental (solid curve) and theoretical (dashed curve) dependence of normalized resistance on reduced temperature for sample A-2. Theory as in Fig. 19.

the width τ_0 of the critical region predicted from Eqs. (2.1) and (2.2), the actual critical region may be wider, as indicated by experimental data for the resistance above T_c.[7–9,38]

The predicted temperature dependence obtained from numerical integration is compared with the data for samples G and A-2 in Figs. 19 and 20, respectively. Only the region $T > T_c$ is plotted. We note that the region near T_c, where $l_+ > l_m$, or $T < T_m$, is given correctly. For the region $T > T_m$, the vortex plasma phase, on the other hand, the theoretical curve rises too rapidly with temperature to agree with the data. Adjusting the unknown constant C_1 by an order of magnitude obviously cannot improve the fit very much, since that would translate the theory curves for $T > T_m$ in the ordinate direction. These log-log plots reveal that the computed curves could fit the data much better if the temperature scale is reduced by about a factor of 3. This suggests that the theoretically computed values of l_+ are too small by a factor of $3^{1/2}$. The theoretical method for computing l_+ is thus shown to be accurate to a factor on the order of unity. Theory is less precisely formulated in the $T > T_c$ region. Also, one has to be concerned with higher-order terms[31] which are neglected in Eqs. (2.1) and (2.2), and which may be important.

VII. CONCLUSIONS

We have performed a test of the equilibrium Kosterlitz and Thouless theory of the vortex-pair unbinding transition with low-frequency measurements on small-area superconducting samples of indium/indium-oxide films. Independent measurements of the vortex-diffusion coefficients give diffusion lengths which are larger than the sample widths. This corroborates the absence of frequency dependence in the inductance and resistance of the small samples. The critical temperature is identified in several ways, through magnetic field dependence and through the values obtained for the reduced stiffness constant, although T_c is not precisely defined for small samples. For $T \lesssim T_c$, the stiffness constant obtained from kinetic inductance and from the exponent of the current-dependent resistance are nearly the same. In the vicinity of T_c we observe the small amount of resistance which comes from a thermally excited free vortex in a sea of thermally excited bound pairs of vortices.

The temperature dependence for the density of the free-vortex plasma phase above T_c has the qualitative exponential inverse-square-root temperature dependence given by the theory. The nonuniversal scaling constant b for $T > T_c$ is a factor of $\sim 3^{1/2}$ smaller than the value which fits the Kosterlitz-Thouless transition for $T \lesssim T_c$. We suspect that this has to do with the neglect of higher-order terms in the solution of the Kosterlitz recursion relations at higher temperatures. The data indicate that $y(l)$ and $K(l)$ vary more slowly near $l \sim l_+$ this is indicated by the solutions of Eqs. (2.1) and (2.2) for $T > T_c$.

The prediction of universality in the jump in electron superfluid density at T_c is confirmed to a precision of about 10%. The uncertainty arises mainly from the 10% scatter in the experimental points, although the fundamental limitation is the finite value of l_m. The fit to the data at finite l_m also reveals the results to be expected as $l_m \rightarrow \infty$. The difference occurs mainly in a small region very close to T_c. To make a significantly better examination of the cusp behavior near T_c requires a much larger value of l_m, say $l \sim 50$. This is an unrealistic extension of the experiment; for superconductors, $l \lesssim \ln(\Lambda/\xi_c) \sim 14$, because of the magnetic screening in a charged superfluid.[39]

The displacement of T_c below T_{c0}, as given by the τ_c parameter, does not follow from a simple analysis of the dirty-limit formula for the penetration depth. The trend of the data shows more rapid reduction of T_c with oxygen doping. Simánek[52] has shown the zero-point phase fluctuations from electrostatic charging in granular films ought to be considered. The influence of electron localization and inhomogeneities[53] have not been taken into account either. Presumably these effects could explain the variations in ϵ_c and C among our samples, since these quantities are determined by extrapolating to short lengths the behavior of the superconducting films measured at macroscopic lengths. A combined renormalization-localization theory is lacking at present.

The Bardeen-Stephen model for flux-flow resistance plays an important role in evaluating the relative experimental length scale r/ξ_c and the thermally excited free-vortex density n_f. Since n_f varies very rapidly with temperature near T_c compared with the vortex diffusivity D (compare low- and high-field regions in Fig. 7), we have assumed that neglecting the temperature dependence of D yields an unimportant systematic error.

ACKNOWLEDGMENTS

This work was begun while one of us (W.I.G.) was a visitor at AT&T Bell Laboratories, and partial support by the National Science Foundation is acknowledged. The SQUID detector was kindly loaned by the Physics Department of Rutgers University. We acknowledge the technical assistance of R. P. Minnich and R. H. Eick, and helpful conversations with J. R. Clem, M. C. Cross, D. S. Fisher, A. M. Goldman, P. C. Hohenberg, D. R. Nelson, and M. Tinkham.

[1]M. R. Beasley, J. E. Mooij, and T. P. Orlando, Phys. Rev. Lett. 42, 1165 (1979).
[2]S. Doniach and B. A. Huberman, Phys. Rev. Lett. 42, 1169 (1979).
[3]L. A. Turkevich, J. Phys. C 12, L385 (1979).
[4]B. I. Halperin and D. R. Nelson, J. Low Temp. Phys. 36, 599 (1979).
[5]A. F. Hebard and A. T. Fiory, Phys. Rev. Lett. 44, 291 (1980).
[6]R. F. Voss, C. M. Knoedler, and P. M. Horn, Phys. Rev. Lett. 45, 1523 (1980).
[7]P. A. Bancel and K. E. Gray, Phys. Rev. Lett. 46, 148 (1981).
[8]K. Epstein, A. M. Goldman, and A. M. Kadin, Phys. Rev. Lett. 47, 534 (1981); Phys. Rev. B 26, 3950 (1982); and (unpublished).
[9]S. A Wolf, D.V. Gubser, W. W. Fuller, J. C. Garland, and R. S. Newrock, Phys. Rev. Lett. 47, 1071 (1981).
[10]P. Minnhagen, Phys. Rev. B 24, 6758 (1981); Phys. Rev. B 27, 2807 (1983).
[11]A. F. Hebard and A. T. Fiory, Physica (Utrecht) 109&110B, 1637 (1982).
[12]B. Giovannini, D. H. Sanchez, and J. L. Berchier, in *Inhomogeneous Superconductors—1979 (Berkeley Springs, WV), Proceedings of the Conference on Inhomogeneous Superconductors,* edited by D. U. Gubser, T. L. Francavilla, S. A. Wolf, and J. R. Lebowitz (AIP, New York, 1979), p. 152.
[13]D. J. Resnick, J. C. Garland, J. T. Boyd, S. Shoemaker, and R. S. Newrock, Phys. Rev. Lett. 47, 1542 (1981).
[14]D. W. Abraham, C. J. Lobb, M. Tinkham, and T. M. Klapwijk, Phys. Rev. B 26, 5268 (1982).
[15]R. F. Voss and R. A. Webb, Phys. Rev. B 25, 3446 (1982).
[16]M. Chester and L. C. Yang, Phys. Rev. Lett. 31, 1377 (1973).
[17]I. Rudnick, Phys. Rev. Lett. 40, 1454 (1978).
[18]D. J. Bishop and J. D. Reppy, Phys. Rev. Lett. 40, 1727 (1978); Phys. Rev. B 22, 5171 (1980).
[19]J. Maps and R. B. Hallock, Phys. Rev. Lett. 47, 1533 (1981).
[20]G. Agnolet, S. L. Teitel and J. D. Reppy, Phys. Rev. Lett. 47, 1537 (1981).
[21]J. K. Bhattachajee and L. Yu, Phys. Rev. B 26, 3946 (1982).
[22]J. Maps and R. B. Hallock, Phys. Rev. B 26, 3979 (1982).
[23]R. A. Joseph and F. M. Gasparini, Phys. Rev. B 26, 3982 (1982).
[24]S. G. Hedge, R. A. Cordery, and W. I. Glaberson, Phys. Rev. B 26, 2690 (1982).
[25]J. M. Kosterlitz and D. J. Thouless, J. Phys. C 6, 1181 (1973).
[26]V. L. Berezinskii, Zh. Eksp. Teor. Fiz. 59, 907 (1970) [Sov. Phys.—JETP 32, 493 (1971)].
[27]J. M. Kosterlitz, J. Phys. C 7, 1046 (1974).
[28]J. M. Kosterlitz and D. J. Thouless, in *Progress in Low Temperature Physics,* edited by D. F. Brewer (North-Holland, Amsterdam, 1978), Vol. VII-B, Chap. 5.
[29]J. V. José, L. P. Kadanoff, S. Kirkpatrick, and D. R. Nelson, Phys. Rev. B 16, 1217 (1977).
[30]A. P. Young, J. Phys. C 11, L453 (1978); Phys. Rev. B 19, 1855 (1979).
[31]R. J. Myerson, Phys. Rev. B 18, 3204 (1978).
[32]B. I. Halperin, in *Proceedings of the Kyoto Summer Institute on Low Dimensional Systems, Kyoto, 1979,* edited by Y. Nagaoka and S. Hikami (Publication Office, Progress of Theoretical Physics, Kyoto, 1979).
[33]D. R. Nelson and J. M. Kosterlitz, Phys. Rev. Lett. 39, 1201 (1977).
[34]B. A. Huberman, R. J. Myerson, and S. Doniach, Phys. Rev. Lett. 40, 12 (1978).
[35]V. Ambegaokar, B. I. Halperin, D. R. Nelson, and E. D. Siggia, Phys. Rev. Lett. 40, 783 (1978); Phys. Rev. B 21, 1806 (1980).
[36]P. Minnhagen, Solid State Commun. 36, 805 (1980).
[37]V. Ambegaokar and S. Teitel, Phys. Rev. B 19, 1667 (1979).
[38]A. F. Hebard and A. T. Fiory, Phys. Rev. Lett. 50, 1603 (1983).
[39]J. Pearl in *Low Temperature Physics—LT9,* edited by J. G. Daunt, D. O. Edwards, F. J. Milford, and M. Yagub (Plenum, New York, 1965), Pt. A, p. 566; Appl. Phys. Lett. 5, 65 (1964).
[40]A. L. Fetter, Phys. Rev. B 22, 1200 (1980).
[41]P. Minnhagen, Phys. Rev. B 23, 5745 (1981).
[42]J. Bardeen and M. J. Stephen, Phys. Rev. 140, A1197, (1965).
[43]J. R. Clem, in *Inhomogenous Superconductors—1979 (Berkeley Springs, WV),* Proceedings of the Conference on Inhomogenous Superconductors, edited by D. U. Gubser, T. L. Francavilla, S. A. Wolf, and J. R. Leibowitz (AIP, New York, 1979) p. 245.
[44]A. F. Hebard and S. Nakahara, Appl. Phys. Lett. 41, 1132 (1982).
[45]R. C. Dynes, J. P. Garno, and J. M. Rowell, Phys. Rev. Lett. 40, 479 (1978).
[46]Model MFP SQUID, S.H.E. Corp., San Diego, CA.
[47]P. M. Horn and R. D. Parks, Phys. Rev. B 4, 2178 (1971).
[48]A. F. Hebard and A. T. Fiory, in *Ordering in Two Dimensions,* edited by S. K. Sinha (North-Holland, Amsterdam, 1980), p. 181; A. T. Fiory and A. F. Hebard, in *Inhomogeneous Superconductors—1979 (Berkeley Springs, WV),* Proceedings of the Conference on Inhomogeneous Superconductors, Ref. 43, p. 293. No electrical contact was made to the sample in the present application of the two-coil technique.
[49]L. G. Aslamosov and A. I. Larkin, Fiz. Tverd. Tela. (Leningrad) 10, 1104 (1968) [Sov. Phys.—Solid State 10, 875 (1968)].
[50]D. S. Fisher, Phys. Rev. B 22, 1190 (1980).
[51]R. G. Petshcek and A. Zippelius, Phys. Rev. B 23, 3483 (1981).
[52]E. Simánek, Phys. Rev. Lett. 45, 1442 (1980).
[53]J. V. José, Phys. Rev. Lett. 46, 1591 (1981).